Perovskite Oxides

Deutsche Ausgabe: DOI: 10.1002/ange.201605561
Internationale Ausgabe: DOI: 10.1002/anie.201605561

Subsurface Space-Charge Dopant Segregation to Compensate Surface Excess Charge in a Perovskite Oxide

Sung-Yoon Chung[+], Si-Young Choi[+], Hye-In Yoon, Hye-Sung Kim, and Hyung Bin Bae*

Abstract: *Since the first prediction by Frenkel, many follow-up studies have been carried out to show the presence of subsurface space-charge layers having the opposite sign to that of the excess charge at the surface, producing overall neutrality in ionic crystals. However, no precise experimental evidence demonstrating how the aliovalent solutes segregate in the space-charge region beneath the surface has been provided over the past several decades. By utilizing atomic-scale imaging and chemical probing in a perovskite oxide, the origin of the surface excess charge at the topmost surface and the position of segregated dopants in the space-charge region is precisely determined. The impact of the space-charge contribution to the dopant distribution near the surface in oxide crystals is explored.*

In contrast to metallic alloys, ionic crystals have a space-charge region near the surface. Since the first postulation by Frenkel,[1] a series of notable works in metal halides have theoretically supported the presence of a space-charge layer to compensate the excess charge at the surface,[2–4] exemplifying plausible defect distributions near the surface in NaCl and AgCl.[3] Based on these studies, the occurrence of the surface charge and its compensating space charge of the opposite sign in pristine ionic crystals (where Schottky-type vacancies are the predominant defects) stems from the difference in the formation free energy between cation and anion vacancies.[2–4] Both the surface potential and the resulting space charge near the surface are thus remarkably altered by impurities in the bulk.[3b] Consequently, the behavior of segregated dopants compared to crystal interfaces (including grain boundaries) is considerably different and is observable,[5–8] depending on the type of aliovalent dopants employed.

A comprehensive study by Yan et al.[9] in 1983 showed that this space-charge effect in ionic crystals is strongly coupled with the elastic-field contribution originating from the size mismatch between the solute and matrix atoms. Similarly, for solutes in metallic crystals such as bismuth (radius, $r = 83$ pm) in copper($r = 29$ pm),[10] and gadolinium ($r = 64$ pm) in magnesium ($r = 12$ pm),[11] a large ionic size difference drives dopants to segregate at the interface of oxides to a significant extent.[12–15] Atomic-scale direct observations of Y^{3+} in Al_2O_3 ($r[Y^{3+}] = 90$ pm; $r[Al^{3+}] = 54$ pm),[12,14] Pr^{3+} in ZnO ($r[Pr^{3+}] = 113$ pm; $r[Zn^{2+}] = 74$ pm),[13] Ca^{2+} in MgO ($r[Ca^{2+}] = 100$ pm; $r[Mg^{2+}] = 72$ pm)[15] are typical examples clearly showing the elastic-field-driven segregation at the core of grain boundaries rather than in the space-charge region near the boundaries in oxides.[16,17] Numerous reports demonstrate segregation instituted by a large mismatch strain of solutes in various material systems. However, little atomic resolution experimental evidence has been provided to elucidate the space-charge-driven solute segregation, even though the space charge is one of the major driving forces for segregation in ionic crystals.

We demonstrate segregation behavior near grain boundaries and near the free surface at the atomic level using Ta^{5+} as a suitable aliovalent dopant in a cubic perovskite titanate, $(Ca_{1/4}Cu_{3/4})TiO_3$. The latter demonstrates multifunctional properties, including exceptionally high permittivity, strong nonlinear I-V behavior, and photocatalysis promoted by visible light.[18] Ta^{5+} ($r = 64$ pm) usually occupies the octahedral Ti^{4+} ($r = 61$ pm) site in perovskite titanates,[19] resulting in a very small difference of less than 5% in ionic size. Consequently, the mismatched strain contribution can be nearly excluded when segregation is observed in our case. To offer both the physical structure and the chemical identification regarding the segregation layers, we utilized high-angle annular dark-field (HAADF) scanning transmission electron microscopy (STEM) and atomic energy-dispersive X-ray spectroscopy (EDS). Density functional theory (DFT) calculations were also used to theoretically verify our findings at the crystal surface.

A polycrystalline $(Ca_{1/4}Cu_{3/4})TiO_3$ sample doped with tantalum was prepared by sintering at high temperature with the aim of observing equilibrium segregation at both the free surface and the grain boundaries. Small pores are contained in this polycrystalline microstructure, and as a result the free surface of $(Ca_{1/4}Cu_{3/4})TiO_3$ crystals in contact with pores can be easily observed as well as grain boundaries, as illustrated in Figure 1a. Figure 1b shows typical HAADF

[*] Prof. S.-Y. Chung,[+] H.-S. Kim
Graduate School of EEWS
Korea Advanced Institute of Science and Technology (KAIST)
Daejeon 34141 (Korea)
E-mail: nalphates@gmail.com
sychung@kaist.ac.kr
Homepage: https://sites.google.com/site/atomicscaledefects/
Dr. S.-Y. Choi[+]
Korea Institute of Materials Science
Changwon 51508 (Korea)
H.-I. Yoon
Department of Materials Science and Engineering
Korea Advanced Institute of Science and Technology (KAIST)
Daejeon 34141 (Korea)
H. B. Bae
KAIST Analysis Center
Korea Advanced Institute of Science and Technology (KAIST)
Daejeon 34141 (Korea)
[+] These authors contributed equally to this work.

Supporting information for this article can be found under: http://dx.doi.org/10.1002/anie.201605561.

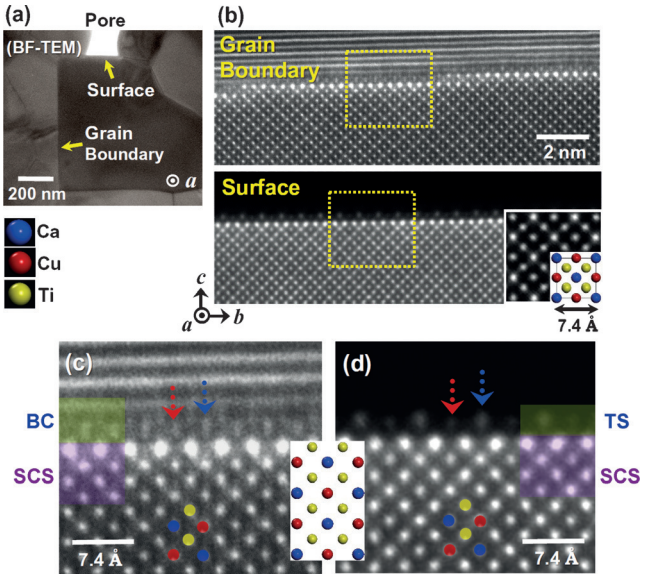

Figure 1. a) A grain with a flat surface and a flat grain boundary. b) Atomic structures for both grain-boundary and surface regions revealed by HAADF-STEM images. Inset: a HAADF image acquired from the bulk. c,d) Magnified images for the regions denoted by a dashed yellow box in (b). The boundary core and the top surface appear to be composed of Ca and Cu columns, as indicated by red and blue arrows. Key: boundary core (BC), top surface (TS), space-charge segregation (SCS).

images demonstrating both a {001} grain boundary and a {001} free surface. A noteworthy feature in both HAADF-STEM images is that very bright atomic columns are readily distinguishable. Based on the highest atomic number of tantalum ($Z=73$) among the four cation compositions (calcium, copper, titanium, and tantalum), this Z-contrast image feature in Figure 1b directly indicates strong tantalum segregation (for additional images of the polycrystalline microstructure see the Supporting Information, Figure S1).

Figures 1c and 1d depict enlargements of the interface regions denoted by a yellow rectangle in Figure 1b, and highlight the key aspect of solute segregation in this study. Notably, the brightest atom column is not located at the core of the grain boundary (Figure 1c) or in the topmost layer of the surface (Figure 1d), as denoted by a green shadow in each image, but appears directly beneath the boundary core and in the subsurface layer. As indicated by a pair of red and blue arrows, the slightly different column intensity and the elongated column shape at the boundary core (Figure 1c) and on the top surface (Figure 1d) imply an atomic arrangement distinct from that in the bulk, although the overall lattice continuity is maintained.

$(Ca_{1/4}Cu_{3/4})TiO_3$ has an ordered configuration of calcium and copper in the A sites of an ABO_3-type perovskite structure (for structural details see the Supporting Information, Figure S2).[20] As copper has a higher Z value ($Z=29$) than that of calcium ($Z=20$) and titanium ($Z=22$), the Cu–Cu columns among the A sites in the [100] projection are easily discriminated from the Ca–Cu columns when ADF images with an enhanced Z-contrast are acquired at a higher collection semiangle (inset of Figure 1b; Supporting Information, Figure S3a).[20] Consequently, as denoted by the atomic array superimposed on each of the images in Figures 1c and 1d, three distinct cation columns, Ca–Cu, Cu–Cu, and Ti–Ti, are precisely identified, demonstrating that most tantalum ions segregate at the first layer of titanium sites with respect to the boundary core and the topmost surface.

An EDS-based chemical analysis was carried out to identify the composition of atomic columns in the surface region. When we analyzed the chemical composition with EDS at comparatively low magnification, a higher intensity of X-ray signals corresponding to tantalum were detected at grain boundaries and the crystal surface in triple pockets (Supporting Information, Figure S4). Figure 2a presents

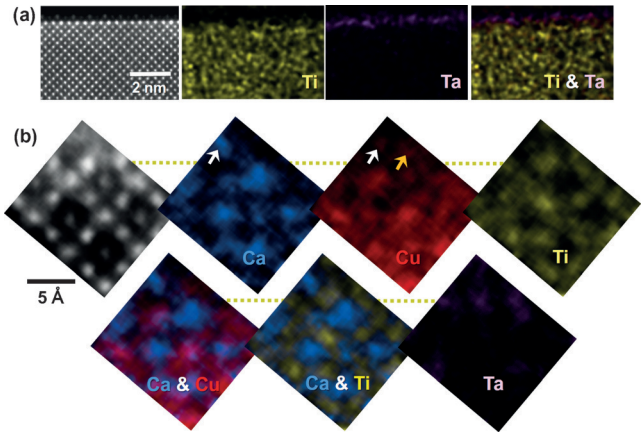

Figure 2. a) EDS maps of Ti and Ta for the region shown in the HAADF image, confirming Ta accumulation near the {001} surface. b) A series of atomic-scale EDS maps acquired in a confined surface region clarifies that most Ta segregates in the subsurface Ti sites (dark yellow dashed lines). The composition of the topmost surface columns consists of Ca–Cu and Cu–only columns (white and orange arrows in the Ca and Cu maps, respectively).

a series of EDS composition maps macroscopically acquired from the surface region shown in the STEM image. In accordance with the bright image intensity in the subsurface layer, the strong X-ray signal of tantalum is easily collected, again confirming its segregation. When we performed a column-by-column analysis of a narrower region, we obtained compositional details at an atomic level. First, each of the atomic columns in the bulk is clearly resolved to enable chemical discrimination between Ca–Cu, Cu–Cu, and Ti–Ti columns (Supporting Information, Figure S3b). Although specimen drift was fairly large during mapping of surface regions, and thereby smearing between columns was more significant than that for the bulk, sufficiently distinguishable atomic-scale composition maps could be acquired for the surface region (Figure 2b). One of the important aspects in this series of maps is that strong tantalum segregation in the subsurface layer is conclusively evident. In each series in Figure 2b a dark yellow dashed line denotes the subsurface tantalum segregation layer at the titanium sites. Furthermore, it was ascertained that the topmost surface consists of calcium/copper (white arrows) and copper-only (orange arrow) columns. Additional sets of EDS maps for

both surface and grain-boundary regions are provided in Figures S5 and S6 (Supporting Information) to ensure the tantalum segregation.

The precise atomic configuration at the surface can be determined by combining the atomically resolved STEM images in Figure 1d and the EDS maps in Figure 2b. DFT calculations informed by the structural information from the experimental results permitted us to ascertain the geometrically optimized surface atomic configuration (Figure 3a; Supporting Information, Figure S7). As calcium and copper are simultaneously detected in the same column at the top surface in the EDS maps in Figure 2b (white arrows), Ca–Cu columns from the bulk appear to be successively maintained up to the surface termination. Consequently, the surface columns denoted by blue arrows in the magnified STEM image, shown in Figure 3b, correspond to Ca–Cu columns. Another notable feature in the enlargement is that the column intensity denoted by a red arrow is much lower than that of the neighboring columns, even though copper is still detected without calcium in the EDS (orange arrow in Figure 2b). This reduction of column intensity, along with the copper signal, thus directly suggests reconstruction of copper in the Cu–Cu columns at the surface, as schematically described in the *c*-projection illustration (right panel) in Figure 3a. In particular, a slight downward shift of the copper surface atom, indicated by a red arrow in the *a*-projection illustration (left panel) in Figure 3a, agrees well with the experimentally obtained image in Figure 3b. The atomic-column image in dark blue shows a HAADF image

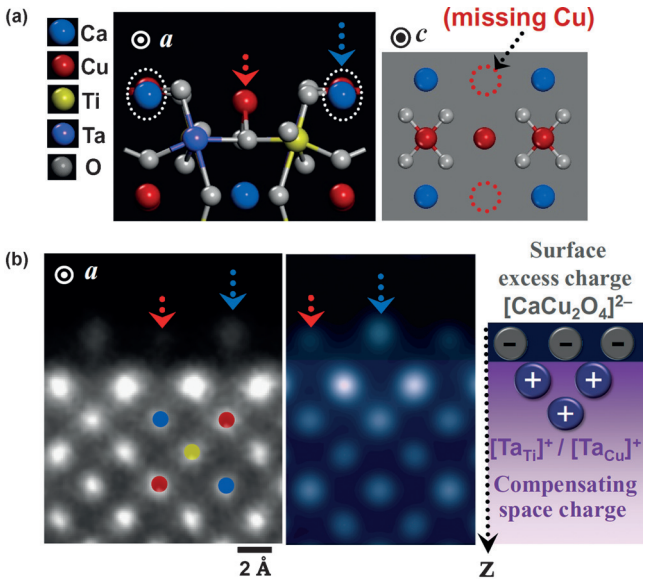

Figure 3. a) A geometrically optimized surface atomic structure based on the HAADF images and the atomic EDS maps. Missing Cu atoms in the Cu column are notable in the surface structure (denoted by dashed red circles). b) The intensity of Ca–Cu surface columns (blues arrows) is higher than that of the neighboring Cu column (red arrow). The simulated STEM image (middle panel) agrees with the experimentally obtained image (left panel). Therefore, as described in the right diagram, the negative surface excess charge ($[CaCu_2O_4]^{2-}$) should be compensated by the positive space charge from the segregated Ta beneath the surface.

simulation with 30% tantalum substitution for titanium sites in the subsurface layer, in line with the real STEM image. Additionally, as can be seen in Figure 3a, the resultant surface atomic configuration is not isotropic. If the surface region is observed in the *b*-projection, the intensity variation between the surface columns should differ from that observed in the *a*-projection (see the configurational depiction at the surface in the Supporting Information, Figure S8a). We could indeed capture an HAADF image that agrees with the surface configuration in the *a*-projection, verifying the validity of the surface atomic structure suggested in our work (Supporting Information, Figure S8b).

The determination of the surface structure allows us to comprehensively understand the origin of surface excess charge. As noted in Figure 3a, the composition of the top surface layer is $[CaCu_2O_4]^{2-}$. This excess negative charge at the surface should be compensated by the positive space charge beneath the top surface, giving overall charge neutrality and resulting in a substantial accumulation of tantalum with an effectively positive charge as a donor dopant in the subsurface region. The diagram shown in Figure 3b describes the charge distribution encompassing the surface excess charge and the compensating space charge of the segregated tantalum. A theoretical prediction of the space charge is fairly difficult—especially in complex oxides with multiple components—because the space-charge model requires essential knowledge concerning the defect formation energies as well as the most favorable type of defects in the bulk lattice.[3] In this regard, this complete atomic-scale description on the origin of the surface charge, and resulting solute segregation on the basis of experimental evidence, is a significant advance that clarifies the role of the space charge as a major driving force for segregation in oxides.

Further to the findings on space-charge segregation, intriguing site occupancy behavior of tantalum was found during STEM observations. Although the majority of added tantalum occupies the titanium sites in the lattice, approximately 10% of tantalum atoms appear to occupy the copper sites, based on the statistical observations obtained by HAADF imaging and atomic EDS mapping (Supporting Information, Figures S9 and S10). Ta^{5+} preferentially occupies an octahedral site, and is coordinated to six oxygen atoms in a perovskite oxide.[19,21] However, as the ionic size of Ti^{4+} and Cu^{2+} in $(Ca_{1/4}Cu_{3/4})TiO_3$ are analogous, some of the Ta^{5+} dopants are observed to occupy the square-planar copper sites (for structural details see the Supporting Information, Note S1 and Figures S9–S11). Therefore, relatively brighter Cu–Cu columns near the grain boundary in Figure 1c and the surface in Figure 1d are understood to stem from the tantalum segregation at the copper sites.

For theoretical verification, we also carried out DFT calculations to compare the lattice stability relative to the tantalum segregation positions in the surface region. Figure 4 shows each of the comparative energy differences with respect to the lattice energy where tantalum is placed in the fourth subsurface titanium layer within a two-unit-cell thickness below the (001) surface. The energy difference listed in Figure 4 is defined by Equation 1.

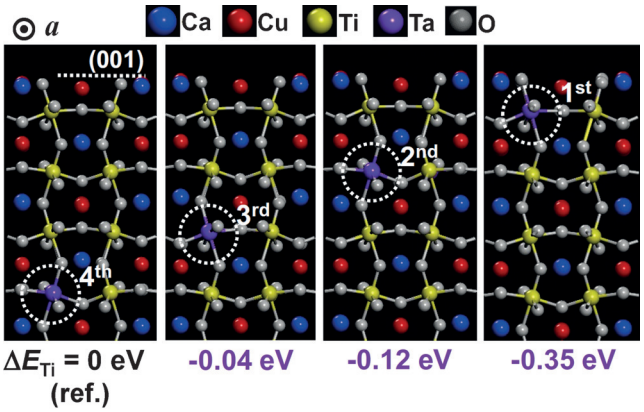

Figure 4. Set of DFT calculations showing relative stabilization of Ta in the Ti sites. The position of Ta substituted in the fourth Ti layer, relative to the surface, is used as a reference for $\Delta E_{Ti} = 0$ eV. As the position of Ta substitution approaches the surface, the relative stabilization energy, ΔE_{Ti}, becomes more negative, supporting the Ta segregation behavior.

$$\Delta E_{Ti} = E(\text{Ta, } n\text{th Ti layer}) - E(\text{Ta, fourth Ti layer}) \quad (1)$$

E is defined as the lattice enthalpy of a supercell containing tantalum near the (001) surface. As the position of tantalum approaches the surface, ΔE_{Ti} has a more negative value, achieving substantial energy stability of -0.35 eV per tantalum atom when the element is placed directly beneath the surface. This set of calculations consistently supports two experimental findings: 1) most tantalum segregates to the first titanium layer as this accumulation is energetically the most favorable configuration; and 2) notable segregation occurs within an approximately two-unit-cell depth scale from the surface, showing a rapid decay to the bulk concentration level (see the STEM image in the Supporting Information, Figure S8b).

Figure 5 compares the relative energy relationship in cases where tantalum is substituted for copper sites. As numerically denoted in Figure 5a, five distinct copper sites near the (001) surface were investigated by using supercell slabs with tantalum segregation in the subsurface titanium layer. Each of the energy differences (ΔE_{Cu}) shown in Figure 5b is defined in a similar manner, by Equation 2.

$$\Delta E_{Cu} = E(\text{Ta, Site } n) - E(\text{Ta, reference Site 1}) \quad (2)$$

E is defined as the lattice enthalpy of a supercell containing tantalum at each site. Compared with the values of ΔE_{Cu} for Sites 1–3 (subsurface copper sites), ΔE_{Cu} for Sites 4 and 5 on the topmost surface exhibits remarkably large positive values (more than $+1.9$ eV), which straightforwardly indicate energetically unfavorable configurations. Therefore, the two sets of DFT calculations in Figures 4 and 5 provide theoretically compelling support for the negative surface charge and compensating positive space charge by tantalum segregation.

A variety of analytical tools are available for a plane-view surface analysis of both topography and chemical composition. We carried out X-ray photoelectron spectroscopy (XPS) and consistently verified both the tantalum segregation in the

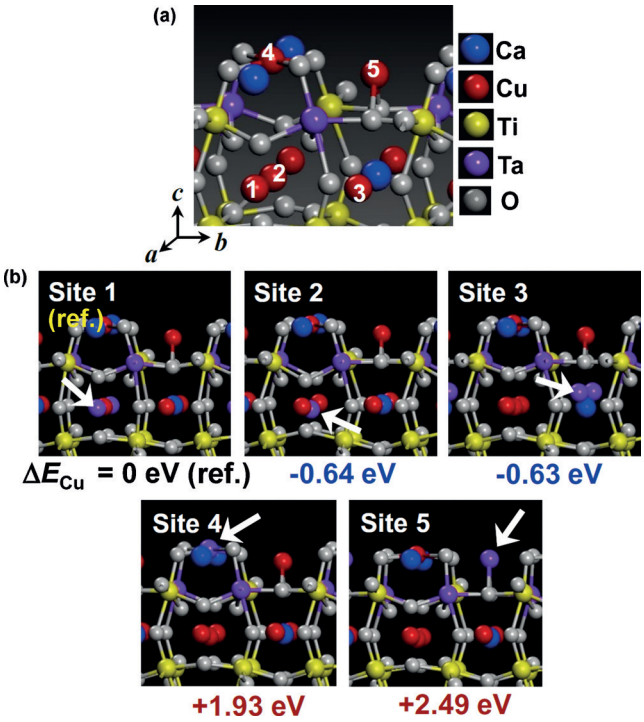

Figure 5. Set of DFT calculations showing relative stabilization of Ta in the surface Cu sites. a) Five distinct Cu sites in the surface region are denoted numerically. b) The position of Ta substituted for Site 1 was used as a reference. In contrast to Sites 1–3, ΔE_{Cu} for Sites 4 and 5 shows significantly large positive values, proving the energetically unfavorable occupancy of Ta on the topmost surface.

surface region and the valence state of Ta^{5+} (see the XPS results in the Supporting Information, Figure S12). However, it remains very challenging to precisely understand the atomic structure and composition beneath the crystal surface.[22] In this regard, this study, which considers both the crystal–crystal internal interface and the free surface, emphasizes the impact of direct subsurface observation at the atomic scale. The findings in the present work also have notable implications regarding the space-charge-driven solute segregation. In contrast to segregation driven by the mismatched elastic strain energy, in which most solutes are confined to boundary cores or the top surface, it is now apparent that the length scale in the space-charge segregation is greater across the interface, as predicted by early theoretical works.[3] However, the segregation width does not appear to extend beyond the level of a few unit cells in our study (see the composition profile in the Supporting Information, Figure S13). The width of a space-charge region is thus believed to be in the range of a few nanometers in perovskite oxides in general, although it may vary depending on the material in the system.

In summary, by using the aliovalent Ta^{5+} dopant, with an ionic size analogous to that of Ti^{4+}, we have identified the precise location of solute segregation in a perovskite titanate near grain boundaries and the free surface. In contrast to segregation typically driven by the large size mismatch of dopants, our study demonstrates that most tantalum cations segregate directly beneath the top surface, clarifying the significant role of space charges as a major driving force for

segregation in oxides. Based on the direct determination of the atomic structure through atomic-resolution *Z*-contrast images and chemical analysis, the origin of negative surface charge was also identified. This work emphasizes the significant correlation of dopant distribution with the local charge distribution near the surface in perovskite oxides.

Acknowledgements

This work was supported by the National Research Foundation of Korea (NRF), grants no. 2014R1A4A1003712 (BRL Program), 2015M2A2A6021169 (Nuclear R&D Program), and 2013M3A6B1078874. S.-Y.C. was also financially supported by the RED&B Project of KAIST.

Keywords: electron microscopy · electrostatic interactions · perovskite phases · segregation · surface chemistry

How to cite: *Angew. Chem. Int. Ed.* **2016**, *55*, 9680–9684
Angew. Chem. **2016**, *128*, 9832–9836

[1] J. Frenkel, *Kinetic Theory of Liquids*, Clarendon Press, Oxford, **1946**.
[2] K. Lehovec, *J. Chem. Phys.* **1953**, *21*, 1123–1128.
[3] a) K. L. Kliewer, J. S. Koehler, *Phys. Rev.* **1965**, *140*, A1226–A1240; b) K. L. Kliewer, *Phys. Rev.* **1965**, *140*, A1241–A1246; c) K. L. Kliewer, *J. Phys. Chem. Solids* **1966**, *27*, 705–717; d) K. L. Kliewer, *J. Phys. Chem. Solids* **1966**, *27*, 719–725.
[4] R. B. Poeppel, J. M. Blakely, *Surf. Sci.* **1969**, *15*, 507–523.
[5] J. A. S. Ikeda, Y.-M. Chiang, A. J. Garratt-Reed, J. B. Vander Sande, *J. Am. Ceram. Soc.* **1993**, *76*, 2447–2459.
[6] S.-Y. Chung, S.-J. L. Kang, V. P. Dravid, *J. Am. Ceram. Soc.* **2002**, *85*, 2805–2810.
[7] W. Lee, H. J. Jung, M. H. Lee, Y.-B. Kim, J. S. Park, R. Sinclair, F. B. Prinz, *Adv. Funct. Mater.* **2012**, *22*, 965–971.
[8] W. Lee, J. W. Han, Y. Chen, Z. Cai, B. Yildiz, *J. Am. Chem. Soc.* **2013**, *135*, 7909–7925.
[9] M. F. Yan, R. M. Cannon, H. K. Bowen, *J. Appl. Phys.* **1983**, *54*, 764–778.
[10] G. Duscher, M. F. Chisholm, U. Alber, M. Rühle, *Nat. Mater.* **2004**, *3*, 621–626.
[11] J. F. Nie, Y. M. Zhu, J. Z. Liu, X. Y. Fang, *Science* **2013**, *340*, 957–960.
[12] J. P. Buban, M. Matsunaga, J. Chen, N. Shibata, W. Y. Ching, T. Yamamoto, Y. Ikuhara, *Science* **2006**, *311*, 212–215.
[13] Y. Sato, J. P. Buban, T. Mizoguchi, N. Shibata, M. Yodogawa, T. Yamamoto, Y. Ikuhara, *Phys. Rev. Lett.* **2006**, *97*, 106802.
[14] N. Shibata, S. D. Findaly, S. Azuma, T. Mizoguchi, T. Yamamoto, Y. Ikuhara, *Nat. Mater.* **2009**, *8*, 654–658.
[15] Z. Wang, M. Saito, K. P. McKenna, L. Gu, S. Tsukimoto, A. L. Shluger, Y. Ikuhara, *Nature* **2011**, *479*, 380–383.
[16] For information on atomic radii, see: B. K. Vainshtein, V. M. Fridkin, V. L. Indenbom, *Structure of Crystals*, 3rd ed., Springer, Berlin, **1995**.
[17] For information on ionic radii, see: R. D. Shannon, *Acta Crystallogr. Sect. A* **1976**, *32*, 751–767.
[18] a) C. C. Homes, T. Vogt, S. M. Shapiro, S. Wakimoto, A. P. Ramirez, *Science* **2001**, *293*, 673–676; b) T. B. Adams, D. C. Sinclair, A. R. West, *Adv. Mater.* **2002**, *14*, 1321–1323; c) S.-Y. Chung, I.-D. Kim, S.-J. L. Kang, *Nat. Mater.* **2004**, *3*, 774–778; d) J. H. Clark, M. S. Dyer, R. G. Palgrave, C. P. Ireland, J. R. Darwent, J. B. Claridge, M. J. Rosseinsky, *J. Am. Chem. Soc.* **2011**, *133*, 1016–1032.
[19] F. S. Galasso, *Perovskites and High T_c Superconductors*, Gordon and Breath Science Publishers, New York, **1990**.
[20] S.-Y. Choi, S.-Y. Chung, T. Yamamoto, Y. Ikuhara, *Adv. Mater.* **2009**, *21*, 885–889.
[21] I. D. Brown, *Chem. Rev.* **2009**, *109*, 6858–6919.
[22] a) M. K. Rose, A. Borg, T. Mitsui, D. F. Ogletree, M. Salmeron, *J. Chem. Phys.* **2001**, *115*, 10927–10934; b) S.-Y. Chung, S.-Y. Choi, T.-H. Kim, S. Lee, *ACS Nano* **2015**, *9*, 850–859.

Received: June 8, 2016
Published online: July 14, 2016

